ORIGINAL PAPER

Long-Term Lubricity of Carbon Nanoparticle Coatings on Periodically Laser-Patterned Metallic Surfaces

Timothy MacLucas[1] · Philipp Leonhard-Trautmann[1] · Sebastian Suarez[1] · Frank Mücklich[1]

Abstract
The lubricity of coatings made from different types of carbon nanoparticles such as carbon onions, carbon nanohorns and carbon nanotubes is investigated on line-patterned AISI 304 stainless-steel substrates using ball-on-disc tribometry over 200,000 sliding cycles. Picosecond direct laser interference patterning is used to create line-patterns on the substrate surfaces which are subsequently coated by electrophoretic deposition. Friction testing is conducted on as-processed surfaces in linear reciprocal mode at a normal load of 100 mN with alumina and 100Cr6 as counter body materials. The resulting wear tracks on the substrates as well as wear scars on the counter bodies are characterized by scanning electron microscopy as well as energy-dispersive X-ray spectroscopy. Tribometry shows that CNTs have the ability to maintain lubricity against both counter body materials. CO and CNH coatings sustain their lubricity against 100Cr6 over the full test duration but fail against alumina. In contrast to alumina, substantial carbon transfer from the substrate surface to 100Cr6 counter body is observed.

Keywords Solid lubricant coatings · Carbon nanotubes · Carbon onions · Carbon nanohorns · Long-term lubricity · Tribometry

1 Introduction

Graphitic nanocarbons represent a material family that includes particles with a variety of different geometries and sizes. Carbon nanotubes (CNT) are among its most prominent members with a proven record of providing effective solid lubrication as a coating [1–4], reinforcing phase in composites [5–8] or lubricant additive [9–11]. Despite different particle morphologies, carbon onions (CO) and carbon nanohorns (CNH) have also demonstrated their ability to significantly reduce friction [12–14], although their tribological properties have not been as intensively researched.

Due to weak adhesion between carbon nanoparticles and metallic substrates, surface texturing is required to prevent their removal from the contact during tribological load, as demonstrated for CNT coatings on stainless steel by Reinert et al. [3]. When combining textured surfaces with carbon nanoparticle coatings, the grooves can act as lubricant reservoirs, providing a steady lubricant supply directly into the contact. Simultaneously, filled reservoirs absorb generated wear particles, thus, preventing them from entering the contact.

Such surface textures can be manufactured in the form of precisely tailored patterns using picosecond direct laser interference patterning (ps-DLIP) [15, 16]. During ps-DLIP, the interference of two or more pulsed sub beams directly on the substrates' surface induces photothermal processes at the interference maxima, resulting in the formation of grooves, grids or dimples with periodicities and aspect ratios that are adjustable to a certain extent. The texture offered by ps-DLIP line-patterns is well suited to carbon nanoparticle coatings, as their aspect ratio is well matched to accommodate and store considerable amounts of particles.

As-processed surfaces are subsequently coated using electrophoretic deposition (EPD), a method for depositing dispersed carbon nanoparticles from a solution onto a conductive substrate by applying a sufficiently high voltage. EPD is well-established for producing homogeneous coatings made from various sp^2-hybridized carbon nanoparticles as it combines simplicity, short processing times, applicability to complex substrate geometries, upscaling potential and cost-effectiveness, while allowing for reproducible deposition results [3, 12, 17–19].

✉ Timothy MacLucas
   timothy.maclucas@uni-saarland.de

1   Department of Materials Science and Engineering, Saarland University, Campus D3.3, 66123 Saarbrücken, Germany

A major criterium for any lubrication system is its ability to maintain lubricity over significant periods of time against different counter body materials without the need for re-supply. In this context, Schäfer et al. conducted tribometry on CNT-coated and cross-patterned austenitic steel substrates over 110,000 cycles at a load of 1 N [1]. The cross-patterns had a structural depth of 1 μm and were manufactured using femto-second direct laser writing. Experiments were conducted on a ball-on-disc tribometer in rotational mode using an alumina counter body (6 mm diameter) at 25 °C and 45% relative humidity. A coefficient of friction (COF) < 0.2 was maintained for about 45,000 cycles before starting to increase considerably.

In this work, coatings made of three different types of carbon nanoparticle on line-patterned stainless-steel platelets are subjected to ball-on-disc friction testing over 200,000 cycles (240 m). The objective is to investigate and compare their respective long-term COF developments against two technically relevant counter body materials: on the one hand, alumina due to its inertness and 100Cr6 as a common bearing steel. Based on the results of MacLucas et al., a low structural depth of 0.23 μm was chosen for the pattern in order to optimize the lubricity of the particle coatings [4].

2 Experimental Section

2.1 Materials

CVD-grown multiwall CNTs with a diameter of 30–85 nm and a length of 10–15 μm purchased at Graphene Supermarket (USA) were utilized. The COs were synthesized by annealing nanodiamonds (NaBond Technologies Co., purity > 98%, particle diameter: 4–8 nm) in a vacuum furnace (model 1100–3580-W1, Thermal Technology Inc.) at 1750 °C for 3 h at a rate of 10 °C/min [20]. Commercially available dahlia-type CNH with a 60–120 nm cluster diameter and a single horn diameter of 2–5 nm (Carbonium SRL, Italy) were used. Mirror-polished AISI 304 austenitic stainless-steel platelets (20×20 mm^2, 1 mm thick) purchased at Brio Kontrollspiegel GmbH (Germany) were used as substrate material. The platelets were thoroughly cleaned with acetone and isopropanol prior to ps-DLIP processing and EPD.

2.2 Picosecond DLIP

A Nd:YAG pulsed laser (Edgewave PX-series InnoSlab) integrated into a RDX 500 nano laser system (Pulsar Photonics GmbH, Germany) was used to fabricate line-patterns on the AISI 304 platelets. The system operates at a wavelength of 532 nm and the samples were processed at 0.5 W. Aforesaid patterns were created with a periodicity (line spacing) of 3.5 μm using two interfering sub beams with a pulse duration of 12 ps. Finally, the patterned surfaces were cleaned by ultrasonication in citric acid, acetone and isopropanol for 15 min each to remove superficial oxide produced during the laser-processing.

2.3 Confocal Laser Scanning Microscopy (CLSM)

An Olympus LEXT OLS4100 confocal laser scanning microscope was utilized to measure the structural depth of the patterns, coating thicknesses. The microscope was operated with a $50 \times$ objective (N.A.: 0.95) at a laser wavelength of 405 nm and a vertical and lateral resolution of 10 nm and 120 nm, respectively. The mean height R_C was used as a measure for the structural depth of the line-patterns over a sampling length of 259 μm. To ensure statistical representation, R_C was determined for 10 different profile lines on images taken at three different spots on the patterned sample surfaces. As the coating thickness cannot be determined directly on the sample surface due to its patterning, separate depositions were made on non-patterned platelets on which deposition parameters were optimized to achieve the target thickness of 4.0–4.5 μm. Subsequently, the optimized parameters were applied to the coating of the patterned surfaces to ensure comparable film thickness.

2.4 Dispersion Preparation and Electrophoretic Deposition

Each dispersion used for electrophoretic deposition contained 70 ml of isopropanol, 10 ml of trimethylamine (ACROS Organics, purity: 99%) and 7 mg of carbon nanoparticle content (0.1 mg/ml solvent). For dispersion, the colloids were subjected to shear mixing (Ultra-Turrax IKA T25), followed by ultrasonication in a Bandelin Sonorex RK514BH (for 10 min each). Subsequently, both the substrate and a comparable platelet representing the counter electrode were immersed in the dispersion and arranged in parallel. After being connected to a DC voltage supply, deposition was conducted at 300 V for 3 min (CNT, CNH) and 4.5 min (CO) to ensure comparable coating thickness.

2.5 Tribometry

A ball-on-disc tribometer (CSM instruments) was used for friction testing in linear reciprocal mode with a stroke length of 0.6 mm at a load of 100 mN. Sliding direction was transversal to that of the line-pattern and performed at a velocity of 1 mm/s. Balls with a diameter of 6 mm from either alumina (Kugel Pompel, GD24) or 100Cr6 steel (Kugel Pompel, Kl.3) were deployed as counter bodies which corresponds to a Hertzian pressure of 0.31 GPa (100Cr6 vs AISI304) and 0.36 GPa (alumina vs AISI304), respectively. Testing was

carried out at room temperature and 4% relative humidity. To attenuate excessive COF oscillation in the graphs, the raw data were slightly smoothed using a Savitzky-Golay filter (50 p). Each sample was measured thrice to ensure statistical representation.

2.6 Wear Track Characterization

A Helios G4 PFIB CXe dual beam work station (Thermo Fisher Scientific, USA) with an integrated EDAX detector for energy-dispersive x-ray spectroscopy (EDS) was employed to characterize the resulting wear tracks at an acceleration voltage of 5 kV and a beam current of 1.6 nA. Chemical mapping was conducted with 8 cumulative frames.

3 Results and Discussion

3.1 Surface Characterization

Figure 1 depicts top view CLSM images of the line-patterned AISI 304 stainless steel substrates after ps-DLIP processing including representative line profiles. As-processed surfaces were subsequently coated with COs (Fig. 1a), CNH (Fig. 1b) and CNTs (Fig. 1c). R_C was determined based on line profiles at different locations to get a representative value for the overall structural depth of the respective pattern. As shown by the images, all surfaces are homogeneously patterned and have close to identical line profiles as well as structural depths.

Figure 2 depicts CO-, CNH- and CNT-coating sections on non-patterned steel surfaces as coating thickness cannot be reliably measured directly on as-processed surfaces. In this case, the profile height of the left (blue rectangle) and right (red rectangle) coating sections are compared to that of an uncoated section in the middle (blue square) on non-patterned and mirror-polished substrates to determine coating thickness. The exact same EPD parameters used for the deposition on non-patterned surfaces were subsequently used to coat the patterned surfaces. The mean thicknesses of all coatings range between 4.2 and 4.4 µm and are, thus, comparable, so that coating thickness can be eliminated as an influencing factor.

3.2 Long-Term Tribological Testing

Figure 3a shows the coefficient of friction (COF) development of the carbon nanoparticle coatings against an alumina
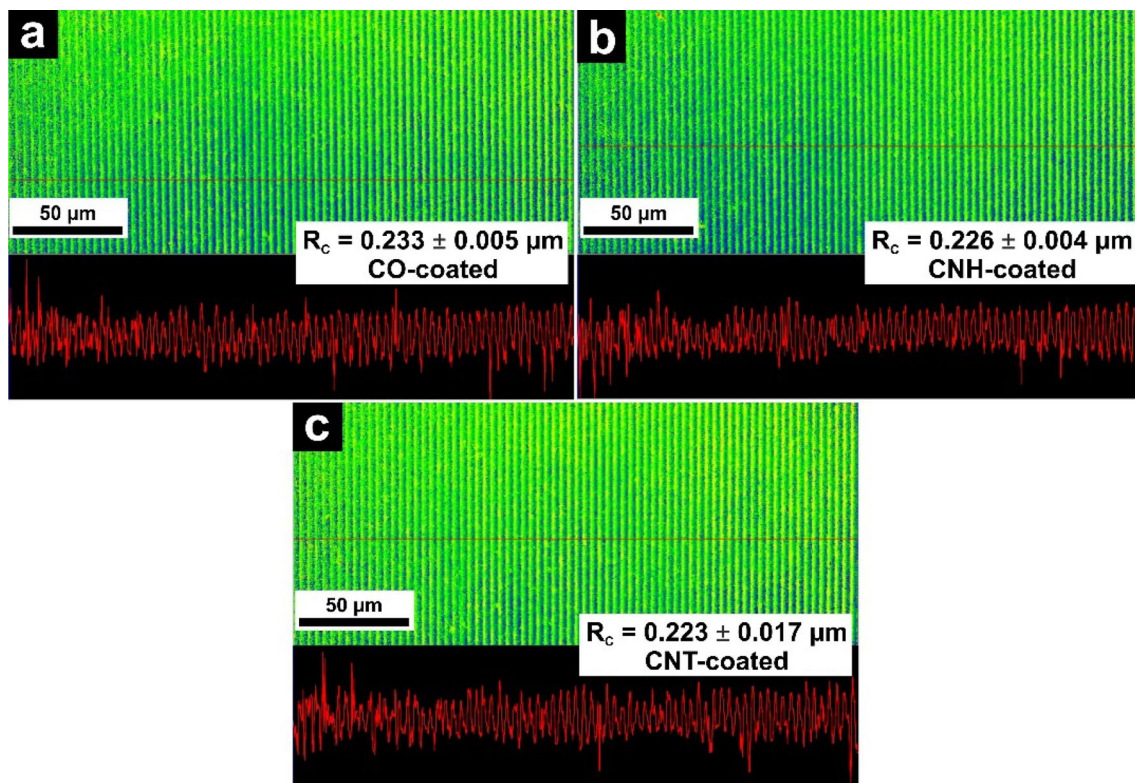

Fig. 1 Top view confocal laser scanning micrographs of the line-patterned AISI 304 substrate which were subsequently coated with **a** COs, **b** CNH and **c** CNTs. In addition to that, the images show representative line profiles and the overall structural depth (R_C) of the respective pattern (Color figure online)
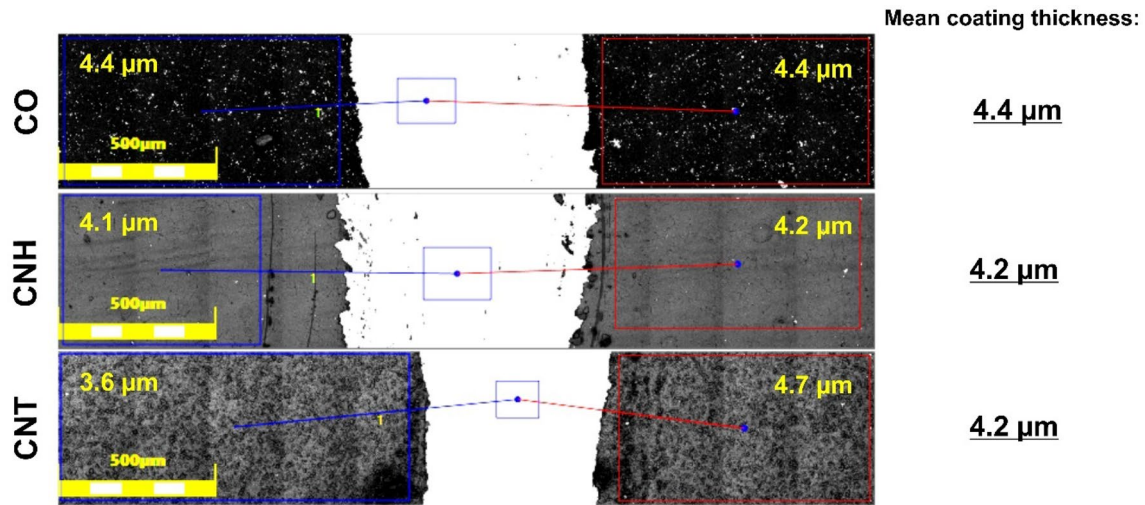
Fig. 2 Confocal laser scanning micrographs of the coatings on non-patterned AISI 304 substrate where the profile height of the marked coating sections (blue rectangles on the left and red rectangles on the right) is compared to that of the uncoated section (blue square in the middle) in order to determine the mean thickness of the CO-, CNH- and CNT-coatings (Color figure online)
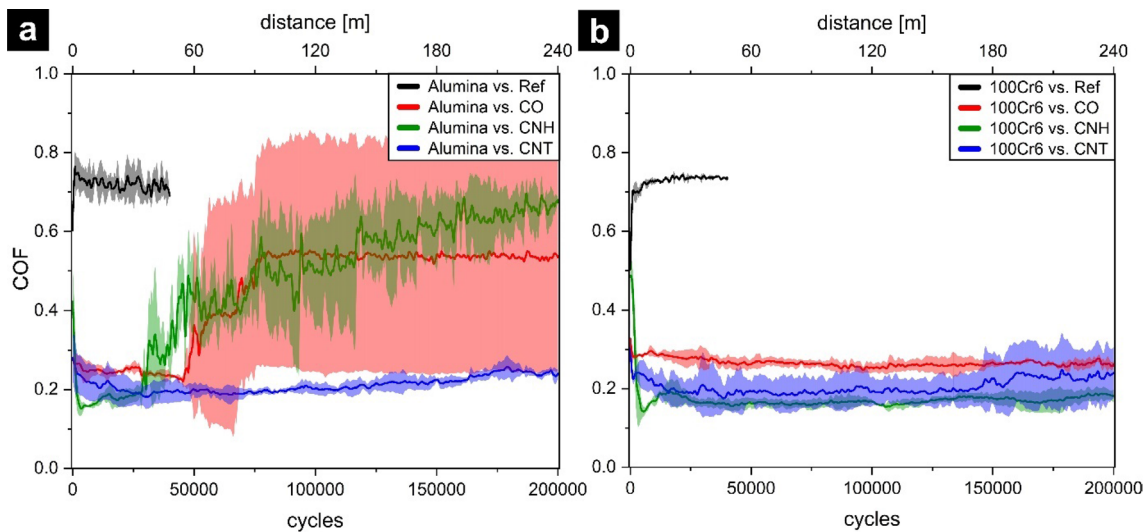

Fig. 3 COF development of CO-, CNT- and CNH-coatings on laser-patterned stainless-steel surfaces against both **a** alumina and **b** 100Cr6 counter bodies (Color figure online)

counter body over 200,000 cycles. A plain uncoated steel surface serves as reference (Ref). Within the initial cycles, its COF rises sharply to 0.76, followed by a slight decrease. According to Blau, this running-in behaviour can be assigned to type b, which is typically observed with non-lubricated metals [21]. After 40,000 cycles, Ref can be considered run-in whilst ranging around 0.70, corresponding well with comparable literature [3]. The COs show a type f behaviour with a subsequent decrease to a COF of 0.22. This is followed by an abrupt and sharp increase until entering steady-state after 78,000 cycles, maintaining a COF of

0.54 throughout the remaining cycles. The COs' extreme standard deviation is due to inconsistent lubricity as during one measurement, lubrication is maintained over the full distance whereas the other two failed prematurely. The running-in of CNH is characterized by a steep initial decline, reaching a COF of 0.17, followed by a steady increase (type h). After 30,000 cycles, the rise increases considerably and the COF continues to climb throughout the test, not reaching a steady-state at all with a final value of 0.66. The likely cause of the observed COF increase is a gradual lubricant depletion, setting in after roughly 30,000 cycles, despite the

surface patterning. Similar to the COs, the CNTs display a distinct type f running-in behaviour with a minimum COF of 0.18 after 30,000 cycles. Subsequently, the COF increases slightly but steadily over the remaining testing period, reaching a final COF of 0.24. CNTs are the only particle type able to maintain lubricity against alumina over the full duration of the friction test.

The COF development of the carbon nanoparticle coatings against a 100Cr6 counter body is presented in Fig. 3b. Unlike alumina, Ref shows a type a running-in and enters steady-stage after approximately 20,000 cycles at 0.73. Resembling a type h, the CO coatings' running-in differs from the measurements against alumina also. Consequently, the COF shows a slight decline and enters steady-state after about 50,000 cycles from which on, it remains around 0.26. The CNHs' running-in strongly resembles that against alumina and can be classified accordingly as type h. In contrast, however, after running-in during which a minimum COF of 0.14 was reached, steady-state is established around 45,000 completed cycles with the COF ranging between 0.16 and 0.18 for the residual test duration. The CNTs running-in remains unchanged by switching the counter body (type f), reaching steady-state lubrication at approximately 45,000 cycles. After 140,000 cycles, the COF starts to increase again, along with the standard deviation, resulting in a final value of 0.24.

In summary, CNTs are able to maintain a lower COF than the COs for almost 150,000 cycles, after which the standard deviations begin to overlap. The CNHs' COF, on the other hand, can be considered significantly lower than that of the COs over the full testing period. Moreover, CNH represent the only particle type able to maintain a COF below 0.20, deemed the threshold for effective solid lubrication by Aouadi et al. [22]. In contrast to tribological testing against the alumina counter body, all carbon nanoparticle coatings were able to sustain lubricity against 100Cr6. It should be noted, that sp^2 carbon nanoparticles are expected to degrade heavily during this type of friction testing as reported specifically for CNTs [1, 3, 5]. It is, therefore, not entirely correct to refer to these particles as such after friction testing, but rather as a tribofilm derived from the respective particle.

3.3 Morphological & Chemical Wear Track Analysis

The SEM image in Fig. 4a shows a heavily worn wear track on the uncoated AISI 304 substrate after rubbing against an alumina counter body (reference) over 40,000 cycles. Adhesion with subsequent delamination represent the main wear mechanisms, however, adhesion is more dominant as indicated by clearly recognizable and characteristic island formation throughout the wear track. Bright green areas throughout the wear track in the corresponding EDS map (Fig. 4b) indicate severe oxidation.

Friction testing against 100Cr6 also leads to heavy wear caused by adhesion (Fig. 4c), however, the resulting wear track is notably wider than its alumina equivalent depicted in Fig. 4a. Since 100Cr6 is softer, permanent deformation is dominant, resulting in a larger contact area. The oxygen map in Fig. 4d reveals severe and uniform oxidation. Furthermore, the particle pile-up at the bottom right of the track in Figs. 4c and d reveals the formation and subsequent removal of oxidic wear particles from the contact.

As previously indicated, the COs inconsistent tribological behaviour suggests fundamentally different lubrication conditions which is confirmed by Fig. 5a–d. The SE micrograph in Fig. 5a shows a fully depleted wear track with pronounced island formation, which is characteristic of adhesion as the dominant wear mechanism. The corresponding EDS map depicted in Fig. 5b verifies complete carbon removal along with severe substrate oxidization, extensive wear particle formation and their subsequent deposition directly next to the wear track. In contrast, Fig. 5c depicts a much narrower and less worn track in which the original surface pattern is well preserved (inset for higher magnification). Considering its chemical map (Fig. 5d), remaining tribofilm can be identified along the edges of the wear track, where minor oxidation has occurred. Of the three CO-coated wear tracks, depletion occurred in two cases while lubrication was maintained in one case. Figure 5e shows island formation once again, therefore, the CNH-coated wear tracks were worn in the same way as the reference or depleted CO tracks: complete carbon removal resulted in severe oxidation, often causing a significant oxide pile-up at the end of the wear track (Fig. 5f). Figure 5g shows the CNT-coated wear track in the centre of which the remnants of the laser-pattern can still be identified and appear to be largely intact (inset for higher magnification). In this case, considerable amounts of CNT-derived carbon remained in the grooves of the pattern and formed large patches, sustaining effective lubrication with no apparent oxidation (Fig. 5h). Bulging at the right end of the wear track demonstrates good coating cohesion.

Unlike alumina, the CO and CNH coatings are not fully removed during friction testing against 100Cr6 (Fig. 6a and c). In the case of COs, the filled grooves are distinct and the line-pattern is well preserved, whereas on the CNH-coated surface, the pattern has been partially worn away (insets for higher magnification). Elemental mapping shows relatively small amounts of CO-derived tribofilm along the edges of the contact area as well as minimum local oxidation at both ends of the wear track (Fig. 6b). In CNH-coated wear tracks, oxidation is more pronounced and can be classified as minor (Fig. 6d). Secondly, the CNH-derived tribofilm is more abundant and spread over a larger area outside of the contact. The remaining carbon is sufficiently abundant for patches to be formed. After rubbing against 100Cr6, the CNT-coated wear track looks similar to its alumina equivalent with the
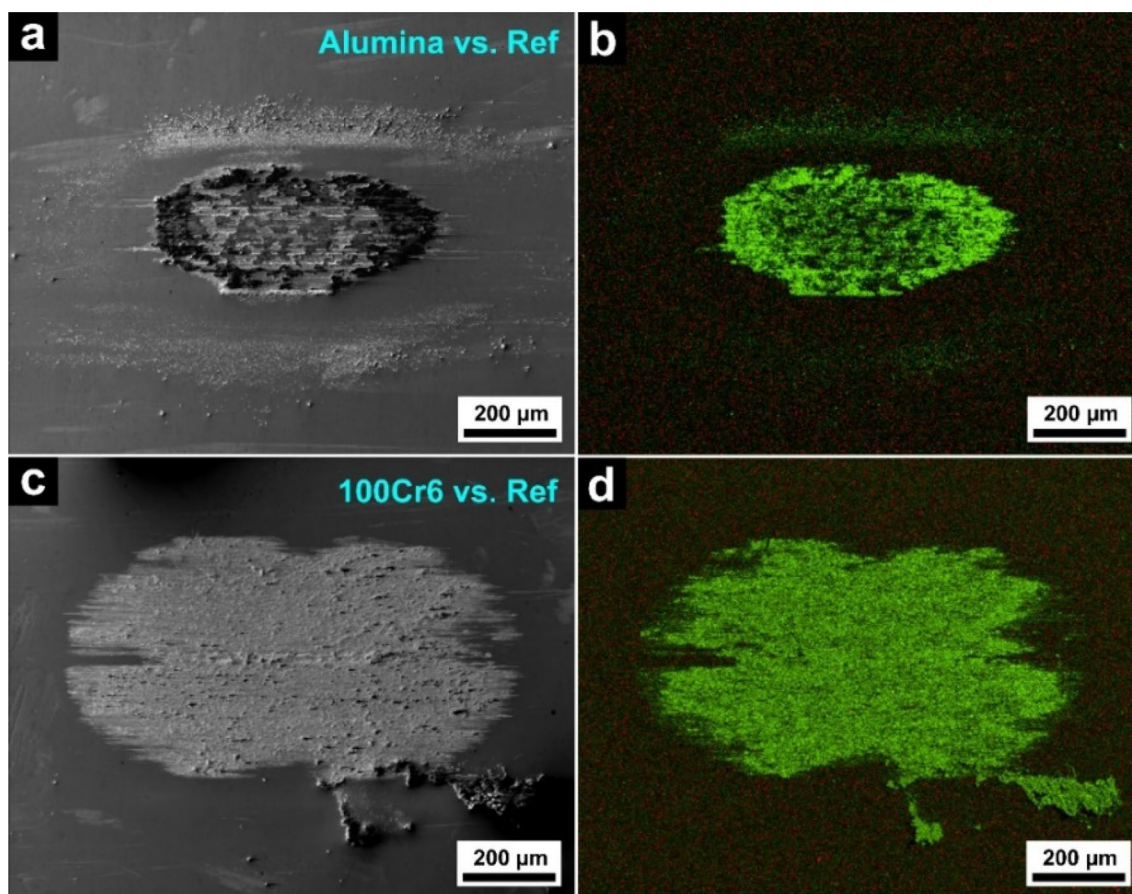
Fig. 4 Scanning electron micrographs of representative uncoated substrates (reference) after rubbing against an **a** alumina and **c** 100Cr6 ball for 40,000 friction cycles. Corresponding EDS maps against **b** alumina and **d** 100Cr6. Green stands for oxygen, red for carbon (Color figure online)

substrate pattern still clearly recognizable (Fig. 6e, inset for higher magnification). The corresponding EDS map reveals significant amounts of carbon, often in the form coherent patches on top of the pattern, with no discernible substrate oxidation (Fig. 6f).

3.4 Material Transfer

Figure 7a shows a typical wear scar on the alumina counter body after friction testing with failed lubrication. The SEM/EDS overlay depicted in Fig. 7b, shows adhesion-induced iron transfer from the substrate wear track to the alumina ball. The thin red film observable in Fig. 7c represents negligible amounts of carbon likely stemming from atmospheric contamination.

After friction testing with successful lubrication, material transfer is either minor (Fig. 8a) or non-detectable (Fig. 8c) as confirmed by the corresponding carbon maps (Fig. 8b and d). Similar to Fig. 7c, the red bands visible in Fig. 8b originate from atmospheric pollution. In case of effective lubrication, the resulting wear scars on the alumina are typically smaller compared to those created by unlubricated friction.

Figure 9a shows EDS mapping of a representative wear scar on a 100Cr6 counter body after tribometry against a reference surface, leading to severe oxidation, as indicated by the bright green areas surrounding the contact. More specifically, oxidic wear particles were generated and subsequently removed from the contact. After testing against CO-, CNH- and CNT-coated surfaces (Fig. 9b–d), the resulting wear scars are smaller compared to that of the reference and oxidation is considerably reduced. The images further demonstrate substantial carbon transfer from the coated substrate to the counter body during tribological load. This phenomenon is particle-independent and can be explained by the formation of covalent bonds between carbon and substrate iron as indicated by MacLucas et al. [4] whereas alumina is far less reactive.

The results have shown that solely CNTs are able to maintain solid lubricity over the full duration of the friction test with no detectable oxidation on any of the substrates against both counter body materials. We believe patch formation to be the principal reason for this behaviour as the presence of patches on top of the pattern effectively separates the sliding surfaces. Due to the

Fig. 5 Scanning electron micrographs of representative wear tracks coated with **a** CO (depl), **c** CO (lubr), **e** CNH and **g** CNT after exposure to 200,000 friction cycles against an alumina ball. Corresponding EDS maps of **b** CO (depl), **d** CO (lubr), **f** CNH and **h** CNT. Green stands for oxygen, red for carbon (Color figure online)
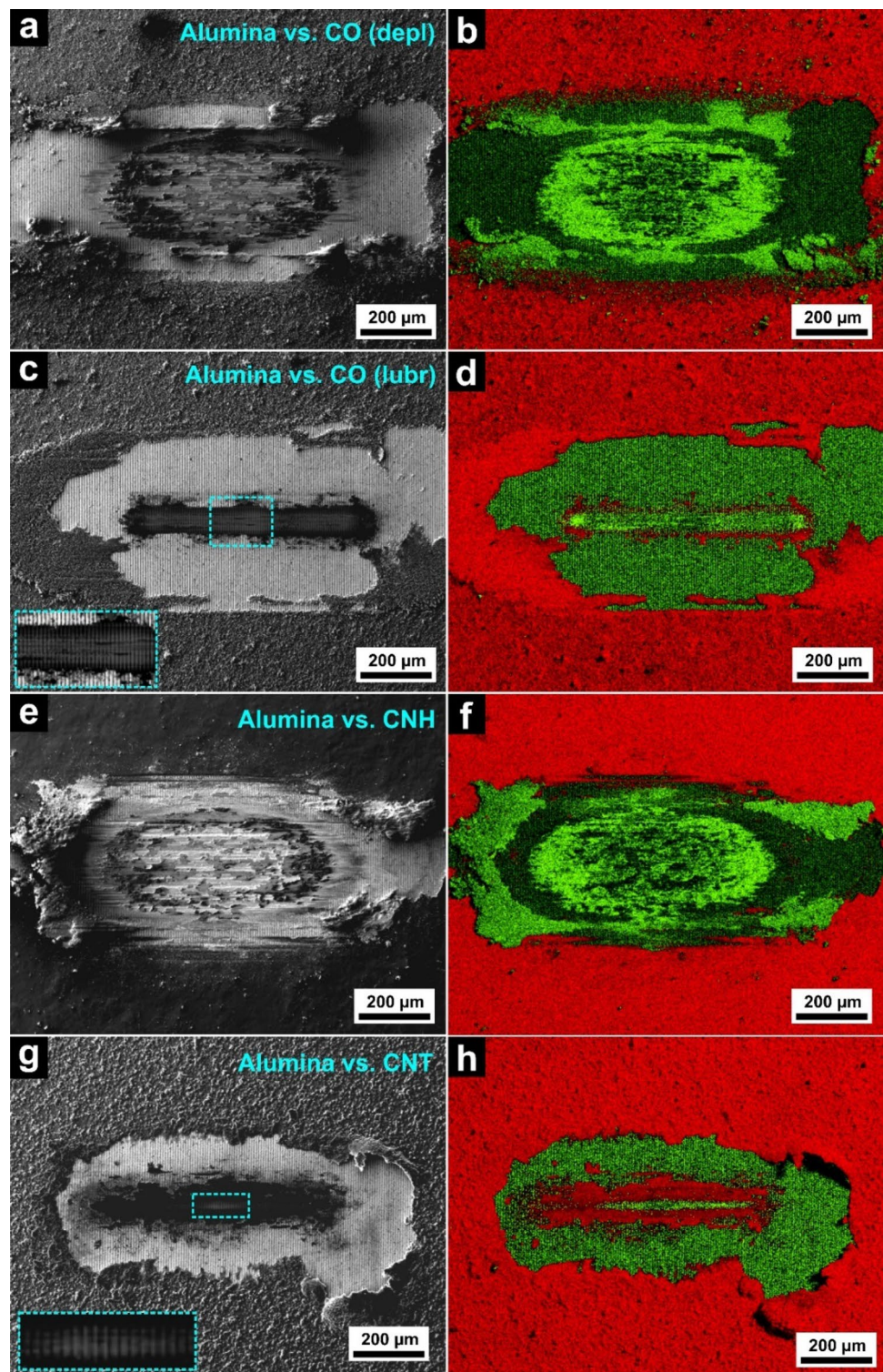
combination of cylindrical morphology and van der Waals interactions, CNTs are able to form strong entanglements. Consequently, their agglomerates are interconnected while embedded in a continuous matrix of CNT coating, thus, facilitating the formation of patches with a strong cohesion. Once formed, those patches are difficult to remove

from the contact as they are likely connected with the underlying CNTs in the grooves and thus anchored in the pattern as illustrated by Fig. 10. Against 100Cr6, CNH are the only coating type able to sustain a mean COF < 0.2 and, thus, effective solid lubrication according to Aouadi et al. throughout the test [22]. In this case, CNH also
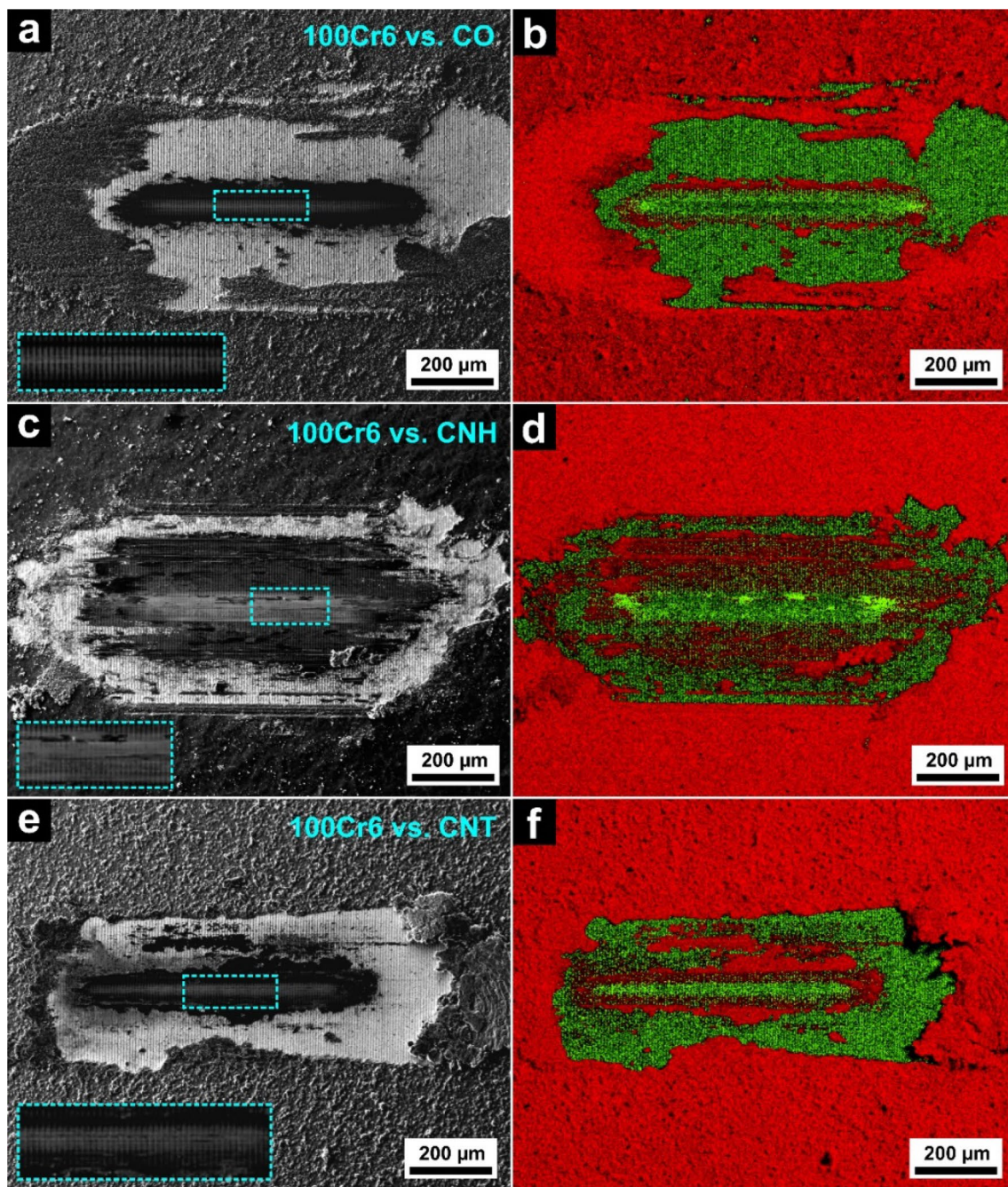
Fig. 6 Scanning electron micrographs of representative wear tracks coated with **a** CO, **c** CNH and **e** CNT after exposure to 200,000 friction cycles against a 100Cr6 ball. Corresponding EDS maps of **b** CO, **d** CNH and **f** CNT. Green stands for oxygen, red for carbon (Color figure online)

form patches, however, compared to CNT patches, they are spread over a larger region which could explain lower COF values as the contact area is increased and thus the contact pressure is reduced. As the morphology of the nanocarbons varies, the character and certain properties of their agglomerates change and so do those of the resulting coatings. Most importantly, individual CNH and CO

agglomerates are not interconnected, hence they are more easily removed than CNTs. The CNH patches are therefore further away from the wear track centre and thus unable to achieve complete separation of the sliding surfaces against a spherical counter body which explains the occurrence of oxidation. EDS analysis of the contact area on the 100Cr6 balls has shown that whenever lubrication is maintained
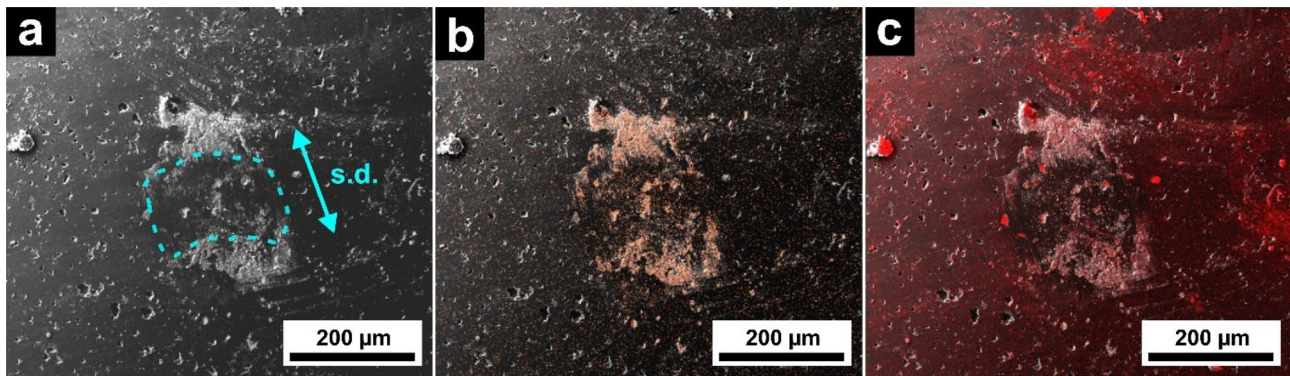
Fig. 7 **a** SE micrograph of a representative wear scar on an alumina ball after 200,000 friction test cycles with failed lubrication. The outline of the wear scar (dotted line) and sliding direction (s.d.) are marked in teal. EDS/SEM overlays for **b** iron (orange) and **c** carbon (red) (Color figure online)
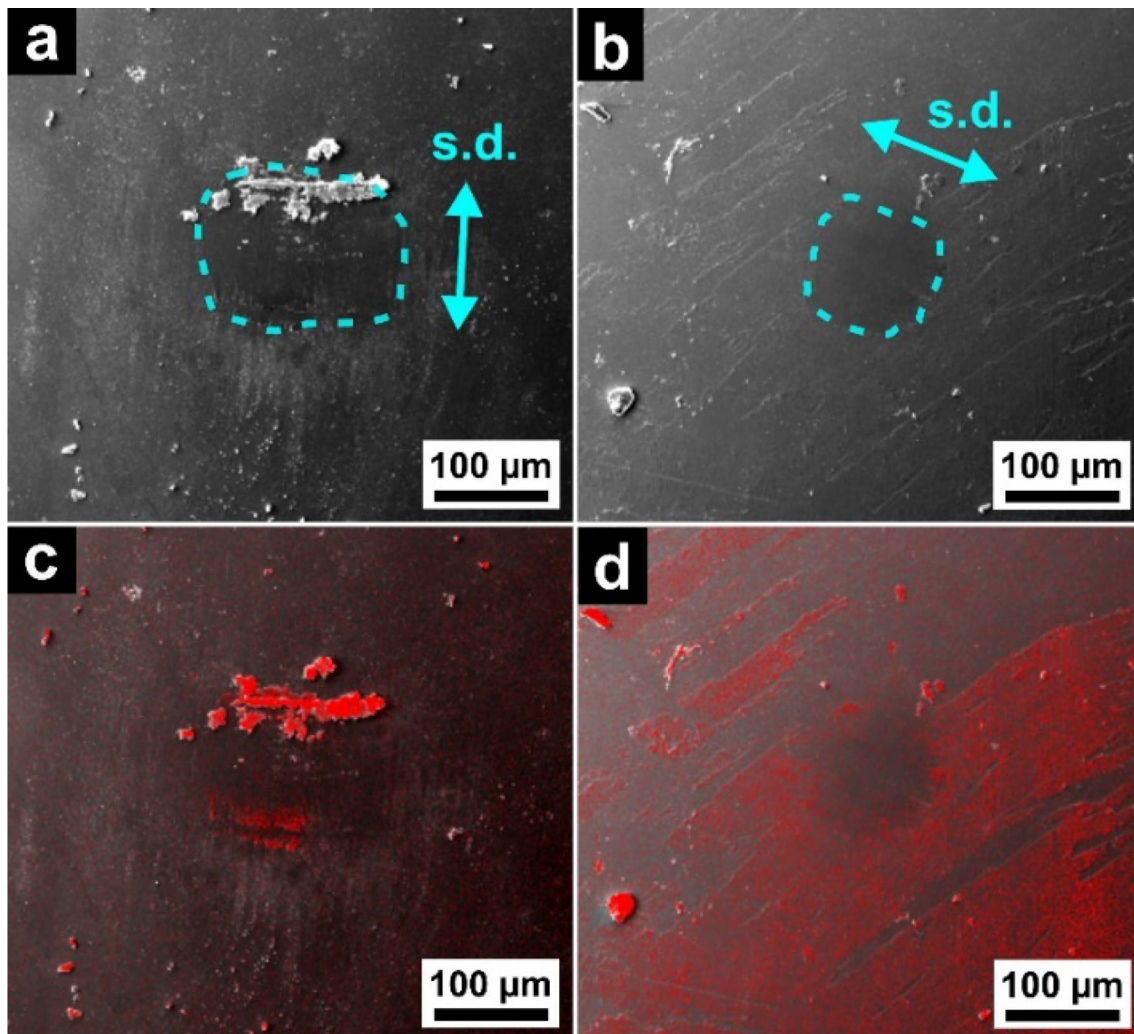

Fig. 8 SE micrographs of representative wear scars on an alumina counter body after 200,000 friction test cycles with functioning lubrication resulting either in **a** minor and **b** no material transfer. The outline of the wear scar (dotted line) and sliding direction (s.d.) are marked in teal. **c** and **d** show corresponding SEM/EDS overlays with red representing carbon (Color figure online)
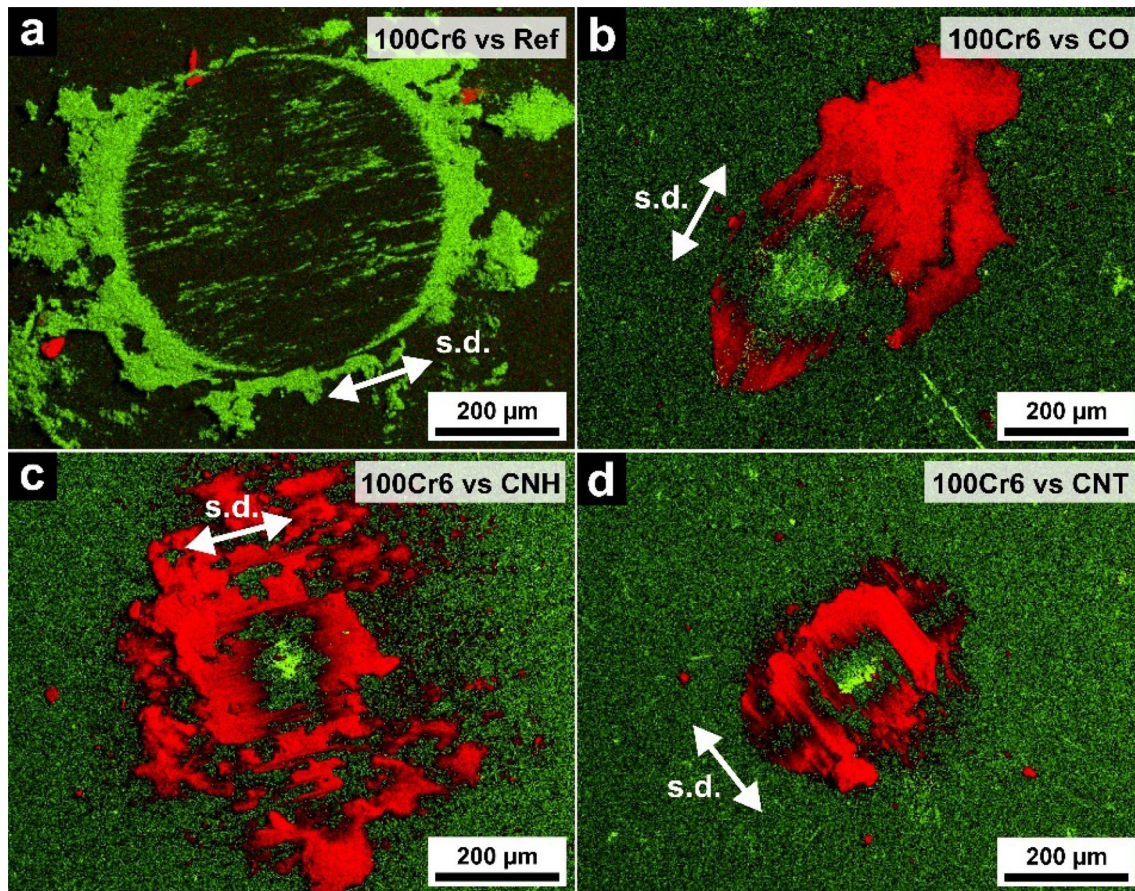
Fig. 9 EDS elemental maps showing representative wear scars on the 100Cr6 balls after rubbing against **a** Ref, **b** CO, **c** CNH and **d** CNT. Green stands for oxygen, red for carbon. The sliding direction (s.d.) is marked by a white arrow (Color figure online)

over the full testing period, significant amounts of carbon are transferred from the coated surface onto the counter body. In contrast, very little carbon, if any, is transferred when sliding against alumina.
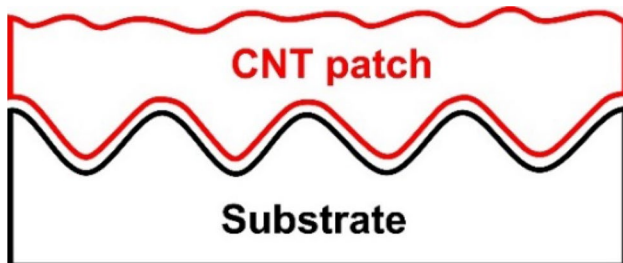

Fig. 10 Schematic cross-section showing CNTs on top of the line-patterned substrate forming cohesive patches with the CNTs stored in the grooves due to counter body pressure during friction testing. As a result, surface adhesion is greatly improved as the patch is interlocked in the grooves (Color figure online)

4 Conclusions

During this study, long-term solid lubrication properties of CO-, CNH- and CNT-coatings on patterned steel substrates were investigated against two technically relevant counter body materials. For that purpose, ball-on-disc tribometry was used in linear reciprocal mode and the resulting substrate wear tracks as well as counter body wear scars were analysed by SEM and EDS. The following three key conclusions can be drawn:

(1) CNT coatings are able to provide long-term lubricity against alumina and 100Cr6 without detectable substrate oxidation. This can be explained by the formation of coherent patches that prevent direct contact of the sliding surfaces.
(2) All particle types were able to lubricate against 100Cr6 over 200,000 friction cycles due to considerable carbon transfer from the patterned/coated surface to the counter body.
(3) CNH achieved the lowest absolute friction against 100Cr6 with a steady-state COF around 0.17

The results presented in this work highlight the impact of particle morphology on the tribological properties of nano-carbon coatings on patterned steel surfaces, despite their physical and chemical similarities.

Declarations

Conflict of interest The authors declare that they have no conflicts of interest.

References

1. Schäfer, C., Reinert, L., MacLucas, T., Grützmacher, P., Merz, R., Mücklich, F., Suarez, S.: Influence of surface design on the solid lubricity of carbon nanotubes-coated steel surfaces. Tribol. Lett. **66**, 1–5 (2018)

2. MacLucas, T., Schütz, S., Suarez, S., Mücklich, F.: Surface protection of austenitic steels by carbon nanotube coatings. Surf. Topogr. Metrol. Prop. **6**, 14005 (2018)

3. Reinert, L., Lasserre, F., Gachot, C., Grützmacher, P., MacLucas, T., Souza, N., Mücklich, F., Suarez, S.: Long-lasting solid lubrication by CNT-coated patterned surfaces. Sci. Rep. **7**, 42873 (2017)

4. MacLucas, T., Daut, L., Grützmacher, P., Guitar, M.A., Presser, V., Gachot, C., Suarez, S., Mücklich, F.: Influence of structural depth of laser-patterned steel surfaces on the solid lubricity of carbon nanoparticle coatings. Friction (2022)

5. Reinert, L., Suárez, S., Rosenkranz, A.: Tribo-mechanisms of carbon nanotubes: friction and wear behavior of CNT-reinforced nickel matrix composites and CNT-coated bulk nickel. Lubricants **4**, 11 (2016)

6. Kim, K.T., Cha, S.I., Hong, S.H.: Hardness and wear resistance of carbon nanotube reinforced Cu matrix nanocomposites. Mater. Sci. Eng. A **449**, 46 (2007)

7. Scharf, T.W., Neira, A., Hwang, J.Y., Tiley, J., Banerjee, R.: Self-lubricating carbon nanotube reinforced nickel matrix composites. J. Appl. Phys. **106**, 013508 (2009)

8. Suárez, S., Rosenkranz, A., Gachot, C., Mücklich, F.: Enhanced tribological properties of MWCNT/Ni bulk composites—influence of processing on friction and wear behaviour. Carbon N. Y. **66**, 164–171 (2014)

9. Kristiansen, K., Zeng, H., Wang, P., Israelachvili, J.N.: Micro-tribology of aqueous carbon nanotube dispersions. Adv. Funct. Mater. **21**, 4555–4564 (2011)

10. Lu, H.F., Fei, B., Xin, J.H., Wang, R.H., Li, L., Guan, W.C.: Synthesis and lubricating performance of a carbon nanotube seeded miniemulsion. Carbon N. Y. **45**, 936–942 (2007)

11. Peng, Y., Hu, Y., Wang, H.: Tribological behaviors of surfactant-functionalized carbon nanotubes as lubricant additive in water. Tribol. Lett. **25**, 247–253 (2007)

12. MacLucas, T., Suarez, S.: On the solid lubricity of electrophoretically deposited carbon nanohorn coatings. Lubricants **7**, 62 (2019)

13. Hirata, A., Igarashi, M., Kaito, T.: Study on solid lubricant properties of carbon onions produced by heat treatment of diamond clusters or particles. Tribol. Int. **37**, 899–905 (2004)

14. Joly-Pottuz, L., Bucholz, E.W., Matsumoto, N., Phillpot, S.R., Sinnott, S.B., Ohmae, N., Martin, J.M.: Friction properties of carbon nano-onions from experiment and computer simulations. Tribol. Lett. **37**, 75–81 (2010)

15. Bieda, M., Siebold, M., Lasagni, A.F.: Fabrication of sub-micron surface structures on copper, stainless steel and titanium using picosecond laser interference patterning. Appl. Surf. Sci. **387**, 175–182 (2016)

16. Aguilar-Morales, A.I., Alamri, S., Lasagni, A.F.: Micro-fabrication of high aspect ratio periodic structures on stainless steel by picosecond direct laser interference patterning. J. Mater. Process. Technol. **252**, 313–321 (2018)

17. Alderete, B., MacLucas, T., Espin, D., Brühl, S.P., Mücklich, F., Suarez, S.: Near superhydrophobic carbon nanotube coatings obtained via electrophoretic deposition on low-alloy steels. Adv. Eng. Mater. **23**, 2001448 (2021)

18. Boccaccini, A.R., Cho, J., Roether, J.A., Thomas, B.J.C., Jane-Minay, E., Shaffer, M.S.P.: Electrophoretic deposition of carbon nanotubes. Carbon N. Y. **44**, 3149–3160 (2006)

19. Thomas, B.J.C., Shaffer, M.S.P., Freeman, S., Koopman, M., Chawla, K.K., Boccaccini, A.R.: Electrophoretic deposition of carbon nanotubes on metallic surfaces. Key Eng. Mater. **314**, 141–146 (2006)

20. Zeiger, M., Jäckel, N., Aslan, M., Weingarth, D., Presser, V.: Understanding structure and porosity of nanodiamond-derived carbon onions. Carbon N. Y. **84**, 584–598 (2015)

21. Blau, P.J.: On the nature of running-in. Tribol. Int. **38**, 1007–1012 (2005)

22. Aouadi, S.M., Gao, H., Martini, A., Scharf, T.W., Muratore, C.: Lubricious oxide coatings for extreme temperature applications: a review. Surf. Coat. Technol. **257**, 266–277 (2014)

Publisher's Note Springer Nature remains neutral with regard to jurisdictional claims in published maps and institutional affiliations.